HHS Public Access

Author manuscript

Laryngoscope. Author manuscript; available in PMC 2023 November 01.

Published in final edited form as:

Laryngoscope. 2022 November ; 132(11): 2142–2147. doi:10.1002/lary.30233.

Stimulated Raman Histology for Rapid Intra-Operative Diagnosis of Sinonasal and Skull Base Tumors

Conall Fitzgerald, MB, MSc[1], **Snjezana Dogan, MD**[2], **Rabih Bou-Nassif, MD**[3], **Tim Mclean, MBBS**[1], **Robbie Woods, MB, MD**[1], **Jennifer R. Cracchiolo, MD**[1], **Ian Ganly, MD, PhD**[1], **Viviane Tabar, MD**[3,*], **Marc A. Cohen, MD, MPH**[1,*]

[1]Head and Neck Service, Department of Surgery, Memorial Sloan Kettering Cancer Center, New York, NY, USA.

[2]Department of Pathology, Memorial Sloan Kettering Cancer Center, New York, NY, USA.

[3]Department of Neurosurgery, Memorial Sloan Kettering Cancer Center, New York, NY, USA.

Abstract

Objective: Intra-operative stimulated Raman histology (SRH) is a novel technology which uses laser spectroscopy and color-matching algorithms to create images similar to formalin-fixed paraffin-embedded (FFPE) section. We aim to assess the accuracy of SRH in a novel range of sinonasal and skull base tumors.

Methods: Select patients undergoing sinonasal and skull base surgery using the *Invenio Imaging™ Nio™* Laser Imaging SRH system between June 2020 and September 2021 were assessed. The SRH images were reviewed for pathologic features similar to frozen section (FS) and FFPE. Time taken for results and diagnostic concordance was assessed.

Results: Sixty-seven SRH images from 7 tumor types in 12 patients were assessed. Pathologies included squamous cell carcinoma, rhabdomyosarcoma, inverted papilloma, adenoid cystic carcinoma, SMARCB1-deficient sinonasal carcinoma, mucosal melanoma, metastatic colonic adenocarcinoma, and meningioma. Tumor was identified in 100% of lesional specimens, with characteristic diagnostic features readily appreciable on SRH. Median time for diagnosis was significantly faster for SRH (4.3 minutes) versus FS (44.5 minutes) (p=<.0001). Where SRH sample site matched precisely to FS (n=32/67, 47.8%), the same diagnosis was confirmed in 93.8%. Sensitivity, specificity, precision, and overall accuracy of SRH was 93.3%, 94.1%, 93.8%, and 93.3%, respectively. Near-perfect concordance was seen between SRH and FS (Cohen's kappa (κ)=0.89).

Conclusion: Stimulated Raman histology can rapidly produce images similar to FFPE H&E in sinonasal and skull base tumors. This technology has the potential to act as an adjunct or alternative to standard FS.

Corresponding Author: Marc A. Cohen, cohenm2@mskcc.org, +1 646 599 2000, Head and Neck Service, Department of Surgery, Memorial Sloan Kettering Cancer Center, New York, NY, USA.

*Denotes co-senior authorship with equal contribution to the manuscript

Level of Evidence: Level IV

Keywords

Skull Base; Sinonasal; Histology; Stimulated Raman Histology

Introduction

Accurate intra-operative histological diagnosis is an essential element of practice in sinonasal and skull base surgery. Assessment of surgical margins to ensure complete tumor excision is typically guided by a combination of anatomic landmarks, pre-operative radiological investigations, intra-operative direct tumor visualization and fresh frozen section analysis[1]. Fresh frozen sampling (FS), which was invented in 1905, presents limitations as it can be time-consuming, labor-intensive and expensive[2,3]. Certain technical limitations also exist, with some pathologies more difficult to interpret on FS, such as sinonasal mucosal melanoma[4].

Determining a diagnosis and establishing margin status in pathologies of the sinonasal cavity and skull base is known to be challenging. Skull base tumors are characterized by their multiple histological subtypes, each with differing clinical behavior[5]. Tumors are frequently excised piece-meal which may distort tumor margins and affect histologic interpretation. Higher rates of positive margins are reported relative to other anatomic subsites, despite a known association with worse overall survival[6]. Given the relative rarity of malignant skull base pathologies, these tumors are typically managed at specialized centers. Identifying improved methods to accurately provide cost-effective, timely intra-operative histology is therefore particularly appealing for the field.

Stimulated Raman histology (SRH) is an emerging technology which permits rapid, intra-operative acquisition of histological images[7]. SRH utilizes Raman laser microspectroscopy to create images similar to formalin-fixed paraffin-embedded (FFPE) hematoxylin and eosin (H&E) sections. To do this, a magnified, depth-resolved image of a tissue specimen is obtained from a sample prepared on a microscopic glass slide. Laser spectroscopy is applied to the sample which detects differences in wavelength based on the tissue constituents, such as lipids, nucleic acids, proteins, and other macromolecules. A coloring algorithm is then applied to each pixel in the image based on the wavelength detected by spectroscopy, which generates a colorized version to replicate a typical FFPE H&E section[8]. Specimens can be assessed at a rate of up to 30 frames per second, permitting near real-time image acquisition[9].

The majority of reported uses for SRH have been in the neurosurgical/central nervous system (CNS) tumors[10]. Sinonasal mucosa is by nature more heterogenous than CNS tissue, containing not just respiratory-type and squamous epithelium, but also minor salivary/seromucinous glands, inflammatory cells, cartilage, or skeletal muscle in the nasopharynx[11]. This more diverse background tissue creates a challenge in interpreting images of sinonasal mucosa produced by SRH. A small number of reports of the application of SRH in skull base surgery have been described, however, the range of pathologies assessed has been limited. In this paper, we describe the novel application of SRH across a broader spectrum of skull base pathologies to assess its potential to aid intra-operative diagnosis.

Materials and Methods

Patient Cohort

Select patients undergoing sinonasal or skull base surgery were enrolled at an academic cancer center from June 2020 – September 2021. Participating specialists were fellowship-trained otolaryngologists, neurosurgeons, and pathologists with a subspecialist interest in sinonasal and skull base surgery. Patient enrollment was at the discretion of the operating surgeons based on clinical need.

Basic patient characteristics and clinicopathologic data were collected pre-operatively. An established pre-operative histological diagnosis was not required for inclusion. No exclusion based on histological subtypes was employed in this exploratory study. Both open and endoscopic sinonasal and skull base procedures were included.

Histologic Assessment

Samples were obtained by the operating surgeon to permit analysis with SRH and/or FS and FFPE. Single or multiple specimens were obtained in each case. Specimens were handed off by the surgeon for immediate SRH analysis in the operating room. Total time required for first image acquisition/result using SRH was recorded to the nearest minute and second. Time to return all FS results was independently recorded to the nearest minute. Images produced by SRH were assessed by a technician and the operating surgeon for features of overt malignancy. In addition, SRH images were reviewed by a specialist head and neck pathologist post-operatively for characteristic tumor features. Where a corresponding sample was available, comparison was made with FS specimens for concordance of diagnosis and presence of characteristic histological features. Digital images of all specimens (SRH, FS and FFPE) were recorded. Samples deemed inadequate for analysis were excluded from the final analysis.

Stimulated Raman Histology Technique

The FDA-approved *Invenio Imaging™ Nio™* Laser Imaging System (Invenio Imaging, Inc., CA, USA) was employed to obtain SRH images under existing Institutional Review Board approval.[12] Sampled tissue was placed on a glass microscopy slide, without additional staining, labelling or treatment. The *Nio™* SRH system uses a dual-wavelength fiber laser system to image the tissue sample at two Raman shifts of 2845cm^{-1} (CH_2) and 2940cm^{-1} (CH_3). Variation in the relative levels of cytoplasm, lipid and protein content in the sampled tissue are detected. A pseudo-coloring algorithm is applied to the images obtained to mimic the appearance of FFPE H&E staining. Pixels in the obtained image which are rich in protein and DNA (measured at 2940cm^{-1}) are colored in a purple hue and pixels rich in lipid (measured at 2845cm^{-1}) are colored in a pink hue. The *Nio™* Laser Imaging System uses a 25x, NA 1.05 water immersion objective microscopic lens and achieves a resolution of <1.25um horizontally and <2.5um axially. Images are acquired as an individual field of view with 1000 pixels per line and ~0.5μm/pixel sample. Images are then stitched into large area mosaics of the specimen to create the final image.

Statistical Assessment

Basic patient characteristic and pathologic data were summarized using descriptive statistics. Comparison was made between the final diagnosis established on SRH and FS using descriptive statistics. Times taken in minutes for result on SRH and FS was recorded. Comparison of time taken for result on SRH versus FS was assessed using the two-sample t-test. Significance was evaluated at the 0.05 alpha level.

Samples on SRH and FS were categorized as 'benign' or 'tumor' tissue to permit calculation of sensitivity, specificity, precision, and overall accuracy of SRH. Cohen's kappa (κ) was calculated for SRH versus FS to assess agreement/concordance between the techniques using the formula = $\frac{Po - Pe}{1 - Pe}$, where Po is the observed agreement between SRH and FS techniques, and Pe is the hypothetical probability of chance agreement between techniques. Outcome data was not included for analysis. Statistical analyses were performed in Stata (version 16, 2019, College Station, TX).

Results

Patient and Tumor Characteristics

Twelve patients with a spectrum of pathologies were enrolled (Table 1). In total, 66.7% were female (n=8) and the median age was 62 years (range 22–84 years). The majority of procedures were completed endoscopically (n=8, 66.7%) for primary pathologies (n=11, 91.7%) and were therapeutic/treatment surgeries (n=9, 75%) rather than diagnostic. Tumor locations were maxillary sinus (n=4, 33.3%), nasal cavity (n=3, 25%), frontal sinus (n=2, 16.7%), ethmoid sinus (n=1, 8.3%), sphenoid sinus (n=1, 8.3%), and pterygopalatine fossa (n=1, 8.3%).

The pathologies assessed using SRH were mostly malignant (n=10, 83.3%) (Table 1). Pathological subtypes included squamous cell carcinoma (SCC) (n=3, 33.3%), rhabdomyosarcoma (n=2, 16.7%), sinonasal papilloma inverted type (n=2, 16.7%), adenoid cystic carcinoma (n=1, 8.3%), SMARCB1-deficient sinonasal carcinoma (n=1, 8.3%), mucosal melanoma (n=1, 8.3%), metastatic colonic adenocarcinoma (n=1, 8.3%), and meningioma (n=1, 8.3%). A total of 67 SRH images were generated (median=4/case) of tumor and marginal tissue. Images were deemed inadequate for analysis and excluded in 6 cases (9%) due to artifact secondary to handling error.

Time-to-Result using Intra-operative Stimulated Raman Histology

The median time to first result for SRH image was 4.3 minutes (258 seconds) (range 3.8 – 6 minutes). The median time to FS results was 44.5 minutes (range 35 – 53 minutes). A statistically significant difference in median reporting times between SRH and FS is noted (p=<.0001), with a 40.2-minute difference between the modalities. It should be noted that FS results were for multiple specimens (median specimens per case = 3.5, range of specimens 1–10) which contributes to the longer time for results compared with SRH where first result is recorded. SRH results were interpreted initially in the operating room by a trained technician and the operating surgeon, prior to separate subsequent specialist review by a

specialist pathologist. Surgeon/user satisfaction was not assessed, however, the workflow was felt to be satisfactory and applicable to sinonasal and skull base surgery.

Accuracy of Diagnosis and Pathological Features Using Stimulated Raman Histology

On postoperative review by a specialist pathologist, tumor diagnosis could be established in 100% of lesional specimens where adequate SRH images were available. In SRH images where sample site matched precisely with the FS sample site (n=32/67, 47.8%), concordance of diagnosis was 93.8%. Discordant results were noted in 6.2% (n=2), where a fragment of the target tumor was seen in either the FS or SRH sample but not both. The sensitivity, specificity, precision, and overall accuracy of SRH images compared with final FS, was 93.3%, 94.1%, 93.3%, and 93.8%, respectively. The SRH technique demonstrated near-perfect agreement with FS with Cohen's kappa (κ) of 0.89.

An example of the initial images generated by SRH is demonstrated in Figure 1. The diagnostic features of SCC seen on SRH images included polygonal tumor cells with dense eosinophilic cytoplasm and loss of polarity, high nuclear/cytoplasmic ratio and enlarged, pleomorphic nuclei and scattered apoptotic tumor cells (Figure 1A). In contrast, benign sinonasal epithelium showed bland cytology with small, round nuclei and bluish cytoplasm consistent with intracellular mucin (Figure 1B). Similarly, the architecture and cytological features of normal minor salivary gland tissue could be easily recognized on SRH (Figure 1C).

Having demonstrated that SRH could confirm diagnosis of malignancy in sinonasal and skull base pathologies, we sought to identify specific pathologic features on SRH images in a broader range of pathologies. In Case 1 (sinonasal papilloma inverted type), cohesive squamous cells and neutrophilic microabscesses (yellow arrows) are seen on the SRH image (Figure 2A), which are similar to those seen on FS and FFPE for the same patient (Figure 2B and 2C). In Case 2 (adenoid cystic carcinoma), cribriform structures filled with basement membrane material (yellow arrows) characteristic of adenoid cystic carcinoma are demonstrated on the SRH image (Figure 2D), and on FS and FFPE (Figure 2E and 2F). In Case 3 (metastatic colorectal adenocarcinoma), cohesive glandular structures (yellow arrows) on SRH (Figure 2G), compare well with those seen with FS and FFPE (Figure 2H and 2I). An example of a sample which could not be interpreted due to artifact caused by specimen handling error prior to image acquisition is shown in Figure 3.

Discussion

Novel adjuncts to traditional intra-operative histological assessment techniques are of particular appeal in sinonasal and skull base surgery, where margin assessment and tumor diagnosis can be challenging. In this study, we highlight application of SRH in the setting of a diverse group of sinonasal and skull base tumors generating 67 SRH images of 7 pathologies. Application of SRH in several of the pathologies in this study is unique. The authors are not aware of any previous application of SRH in sinonasal salivary gland malignancy, metastatic colonic adenocarcinoma to the sinonasal tract, sinonasal papilloma inverted type or sinonasal rhabdomyosarcoma. In addition, we report what we believe to be the first application of SRH in open craniofacial/sinonasal surgery. We highlight

characteristic appearances of these pathologies on SRH images. Our findings demonstrate the potential to obtain rapid, intra-operative FFPE H&E-like SRH images in sinonasal and skull base surgery and the potential utility of this technology in this area. Benefits in terms of reduced operative time, enhanced operating room workflow, and reduced labor time for in-demand pathologists may be significant.

Since the early description of stimulated Raman scattering (SRS) microscopy by Freudiger et al. in 2008, technologies have been adapted to allow intra-operative assessment of histological specimens, so-called stimulated Raman histology (SRH)[7,13]. The use of SRH has been largely confined to the neurosurgical setting to assess CNS pathologies where a more homogenous background tissue surrounds tumors. Several high-quality reports have compared imaging using SRH devices versus FS and FFPE. Orringer et al. described in 2017 the application of SRH in 101 neurosurgical patients[14]. Utilizing SRS technology, they successfully created images with virtual H&E staining for intra-operative assessment. They reported excellent concordance with FFPE (Cohen's kappa, κ>0.89), and diagnostic accuracy exceeding 92% in mostly glioblastoma, astrocytoma and oligodendroglioma cases.

Eichberg et al. reported a prospective blinded cohort study of 82 patients undergoing resection of CNS tumors, finding the mean time to diagnosis was 30.5 minutes faster (p=<.0001) for SRH compared to FS (p=<.0001). Diagnostic concordance was reported in 91.5% of cases (κ=0.834, p=<.0001) between SRH and FFPE, and 91.5% between FS and FFPE (κ=0.894, p=<.0001)[15]. Hollon et al. in 2020 applied machine learning technologies using deep convolutional neural network training on over 2.5 million SRH images from 278 patients to assess the diagnostic accuracy between artificial intelligence and pathologists in a multi-center non-inferiority trial.[8] In their study, the largest SRH clinical trial published to date, the SRH device demonstrated marginally higher overall diagnostic accuracy compared with FFPE assessment (95.6% versus 93.9% diagnostic accuracy, respectively). Further machine learning studies have explored how SRH could interpret diagnosis[16].

A study of SRH reporting skull base pathologies was published by Shin et al. in 2019, and included 9 meningiomas, 3 schwannomas, and 1 chordoma, chondroma, chondrosarcoma, somatotroph adenoma, and craniopharyngioma, respectively[17]. They describe pathologies arising in anatomic locations such as the clinoid process, petrous apex, cerebellopontine angle, clivus, planum sphenoidale and other locations, but did not report any sinonasal cases. Hoesli et al. applied SRH in the head and neck, including oral cavity and larynx, demonstrating excellent sensitivity in diagnosing malignancy[18]. The application of SRH has been expanded to other tissue types, including skin, gastric, pharyngeal, and laryngeal mucosa, highlighting additional potential applications outside the CNS.[19–22] The authors of this study anticipate an uptake of the application of SRH to other anatomic locations and pathologies where rapid intra-operative diagnosis is desirable.

We demonstrate in our study a high degree of diagnostic accuracy for SRH in the setting of skull base and sinonasal pathologies with sensitivity and specificity of 93.3% and 94.1%, respectively. Excellent concordance of diagnosis is seen between SRH and FS on matching samples if the tested sample was of adequate quality and quantity. Potential challenges do exist, including processing artifacts and under sampling due to small volume of disease,

although these limitations also exist with intra-operative FS diagnosis. Nevertheless, we demonstrate SRH to be significantly faster than traditional FS techniques in providing intra-operative diagnosis, on average 40 minutes faster per case. The cost of frozen section analysis in head and neck surgery has been reported as $3,123 per case in earlier studies[23]. Identifying technologies aimed at reducing this cost would be beneficial. The argument for the use of SRH in complement with traditional FS techniques guided by a specialist pathologist appears well-made. SRH may offer particular benefit in skull base and sinonasal pathologies where multiple FS may be required to confirm margin status and where margin status affects survival, recurrence and requirement for adjuvant treatment[24]. Whether these images alone could be the basis of decision-making in the operating theater remains unclear until further studies are performed, as certain limitations of SRH do exist.

The diverse background tissue of the sinonasal cavity and skull base creates a challenge in interpreting images of sinonasal mucosa produced by SRH. While we demonstrate that many features of malignancy can be recognized on SRH images, including loss of polarity, high nuclear/cytoplasmic ratio and nuclear pleomorphism in SCC, other diagnostic features that can be assessed on FS or FFPE may not be readily apparent in SRH images, such as the features of a mitotic figure versus apoptotic cell. If specimens are divided for assessment with both SRH and FS, differences may exist in the tissue sent to either modality. Using both modalities also duplicates the work being performed, negating the potential benefits of the rapid intra-operative results provided by SRH. Designating tissue as malignant versus benign only may be a more realistic application at this time than making exact diagnosis intra-operatively using SRH alone. Discerning dysplasia and carcinoma-in-situ from malignancy on small fragments of tissue may also present a challenge with SRH, as with FS. The assessment of intra-operative margin status in skull base surgery is a much-debated topic. For these reasons, further investigation is required to understand the role of this promising technology and its potential application in sinonasal and skull base surgery. Finally, a thorough cost-benefit analysis of this technology would be beneficial to conduct in future.

In addition to the limitations of the SRH technique, there a number of limitations of this study, most notably that the sample size is small. The pathologies we describe are rare and the application of SRH in this setting is novel therefore multi-institutional collaboration in a prospective study would likely be required to expand the available data for sinonasal and skull base pathologies. Our study did not obtain matching samples for SRH, FS and FFPE in all cases, which limits our ability to make comparisons regarding diagnostic concordance for all samples obtained and against FFPE. This manuscript focuses on comparing intra-operative modalities of SRH and FS only. We analyze the time to first SRH result versus overall time for FS results due to local reporting practices, which may affect interpretation of time-to-results data. The technology is novel for both the surgeons and pathologists as this device is available only in a limited number of centers in the USA at present. Enhanced familiarity with the technology and its capabilities could improve diagnostic accuracy, scope of application and time to results. All specimens in our study were assessed by a specialist head and neck pathologist with experience in skull base pathology, which is not feasible in all centers and may alter the final results.

Conclusion

Intra-operative images with features comparable to FFPE H&E section can be rapidly produced using SRH in sinonasal and skull base pathologies. The applications of SRH in endoscopic sinonasal and skull base surgery are broader than previously described. SRH may provide efficiencies compared with traditional FS techniques. Further investigation is required to establish the scope of practice for this technology as an adjunct or alternative to FS.

Funding and Conflict of Interest Disclosure:

This study was partly funded by the NIH/NCI Cancer Center Support Grant P30 CA008748.

Abbreviations:

SRS	stimulated Raman scattering
SRH	stimulated Raman histology
FS	fresh frozen sampling
FFPE	formalin-fixed, paraffin-embedded
H&E	hematoxylin and eosin
CNS	central nervous system

References

1. Lund VJ, Stammberger H, Nicolai P, et al. European position paper on endoscopic management of tumours of the nose, paranasal sinuses and skull base. Rhinol Suppl. 2010;22(2):1–143. [PubMed: 20502772]
2. Gal AA, Cagle PT. The 100-year anniversary of the description of the frozen section procedure. Jama. 2005;294(24):3135–3137. [PubMed: 16380595]
3. Jaafar H. Intra-operative frozen section consultation: concepts, applications and limitations. The Malaysian journal of medical sciences: MJMS. 2006;13(1):4. [PubMed: 22589584]
4. Sayed Z, Migliacci JC, Cracchiolo JR, et al. Association of surgical approach and margin status with oncologic outcomes following gross total resection for sinonasal melanoma. JAMA otolaryngology–head & neck surgery. 2017;143(12):1220–1227. [PubMed: 29049462]
5. Patel SG, Singh B, Polluri A, et al. Craniofacial surgery for malignant skull base tumors: report of an international collaborative study. Cancer: Interdisciplinary International Journal of the American Cancer Society. 2003;98(6):1179–1187.
6. Suarez C, Llorente JL, Fernandez De Leon R, Maseda E, Lopez A. Prognostic factors in sinonasal tumors involving the anterior skull base. Head Neck. Feb 2004;26(2):136–44. doi:10.1002/hed.10358 [PubMed: 14762882]
7. Freudiger CW, Yang W, Holtom GR, Peyghambarian N, Xie XS, Kieu KQ. Stimulated Raman scattering microscopy with a robust fibre laser source. Nature photonics. 2014;8(2):153–159. [PubMed: 25313312]
8. Hollon TC, Pandian B, Adapa AR, et al. Near real-time intraoperative brain tumor diagnosis using stimulated Raman histology and deep neural networks. Nat Med. Jan 2020;26(1):52–58. doi:10.1038/s41591-019-0715-9 [PubMed: 31907460]

9. Saar BG, Freudiger CW, Reichman J, Stanley CM, Holtom GR, Xie XS. Video-rate molecular imaging in vivo with stimulated Raman scattering. Science. Dec 3 2010;330(6009):1368–70. doi:10.1126/science.1197236 [PubMed: 21127249]
10. Hollon T, Lewis S, Freudiger CW, Sunney Xie X, Orringer DA. Improving the accuracy of brain tumor surgery via Raman-based technology. Neurosurg Focus. Mar 2016;40(3):E9. doi:10.3171/2015.12.FOCUS15557
11. Franchi A. Pathology of sinonasal tumors and tumor-like lesions. Springer; 2019.
12. https://www.invenio-imaging.com/.InvenioImagingNioLaserImagingSystem. Accessed November 11, 2021.
13. Freudiger CW, Min W, Saar BG, et al. Label-free biomedical imaging with high sensitivity by stimulated Raman scattering microscopy. Science. 2008;322(5909):1857–1861. [PubMed: 19095943]
14. Orringer DA, Pandian B, Niknafs YS, et al. Rapid intraoperative histology of unprocessed surgical specimens via fibre-laser-based stimulated Raman scattering microscopy. Nature biomedical engineering. 2017;1(2):1–13.
15. Eichberg DG, Shah AH, Di L, et al. Stimulated Raman histology for rapid and accurate intraoperative diagnosis of CNS tumors: prospective blinded study. J Neurosurg. Dec 6 2019:1–7. doi:10.3171/2019.9.JNS192075
16. Khalsa SSS, Hollon TC, Adapa A, et al. Automated histologic diagnosis of CNS tumors with machine learning. CNS Oncol. Jun 2020;9(2):CNS56. doi:10.2217/cns-2020-0003 [PubMed: 32602745]
17. Shin KS, Francis AT, Hill AH, et al. Intraoperative assessment of skull base tumors using stimulated Raman scattering microscopy. Sci Rep. Dec 31 2019;9(1):20392. doi:10.1038/s41598-019-56932-8 [PubMed: 31892723]
18. Hoesli RC, Orringer DA, McHugh JB, Spector ME. Coherent Raman Scattering Microscopy for Evaluation of Head and Neck Carcinoma. Otolaryngol Head Neck Surg. Sep 2017;157(3):448–453. doi:10.1177/0194599817700388 [PubMed: 28397572]
19. Zhang L, Wu Y, Zheng B, et al. Rapid histology of laryngeal squamous cell carcinoma with deep-learning based stimulated Raman scattering microscopy. Theranostics. 2019;9(9):2541–2554. doi:10.7150/thno.32655 [PubMed: 31131052]
20. Sarri B, Canonge R, Audier X, et al. Fast stimulated Raman and second harmonic generation imaging for intraoperative gastro-intestinal cancer detection. Sci Rep. Jul 11 2019;9(1):10052. doi:10.1038/s41598-019-46489-x [PubMed: 31296917]
21. Hakert H, Eibl M, Tillich M, et al. Time-encoded stimulated Raman scattering microscopy of tumorous human pharynx tissue in the fingerprint region from 1500–1800 cm(−1). Opt Lett. Jul 15 2021;46(14):3456–3459. doi:10.1364/OL.424726 [PubMed: 34264237]
22. Mittal R, Balu M, Krasieva T, et al. Evaluation of stimulated Raman scattering microscopy for identifying squamous cell carcinoma in human skin. Lasers Surg Med. Oct 2013;45(8):496–502. doi:10.1002/lsm.22168 [PubMed: 23996592]
23. DiNardo LJ, Lin J, Karageorge LS, Powers CN. Accuracy, utility, and cost of frozen section margins in head and neck cancer surgery. The Laryngoscope. 2000;110(10):1773–1776. [PubMed: 11037842]
24. Eichberg DG, Ivan ME, Komotar RJ. Intraoperative Stimulated Raman Histology for Anterior Skull Base Tumor Margins: Can We Improve Patient Survival and Time to Recurrence? World Neurosurg. May 2021;149:265–266. doi:10.1016/j.wneu.2021.03.012 [PubMed: 33940674]

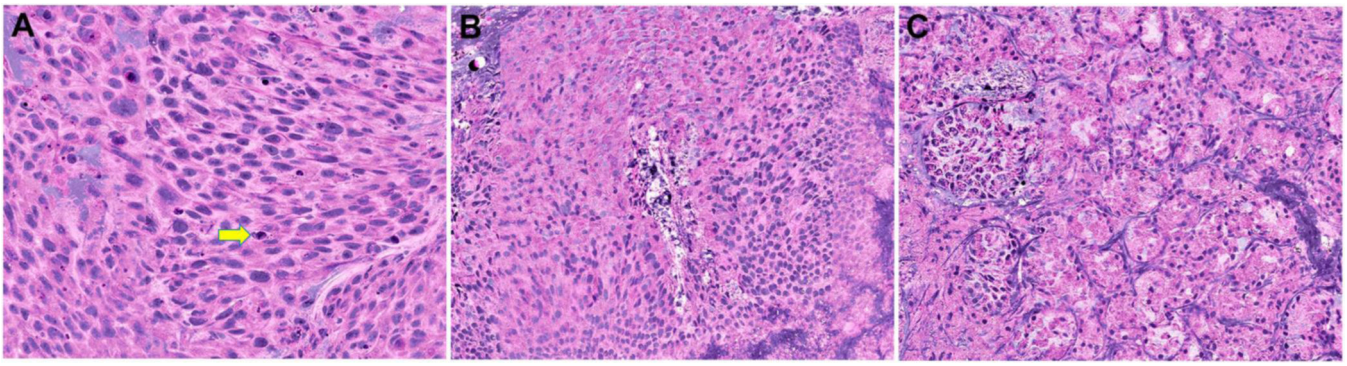

Figure 1:
Stimulated Raman histology images demonstrating (A) sinonasal squamous cell carcinoma (yellow arrow highlights an apoptotic tumor cell) (B) benign (normal) sinonasal epithelium and (C) minor salivary/seromucinous glands.

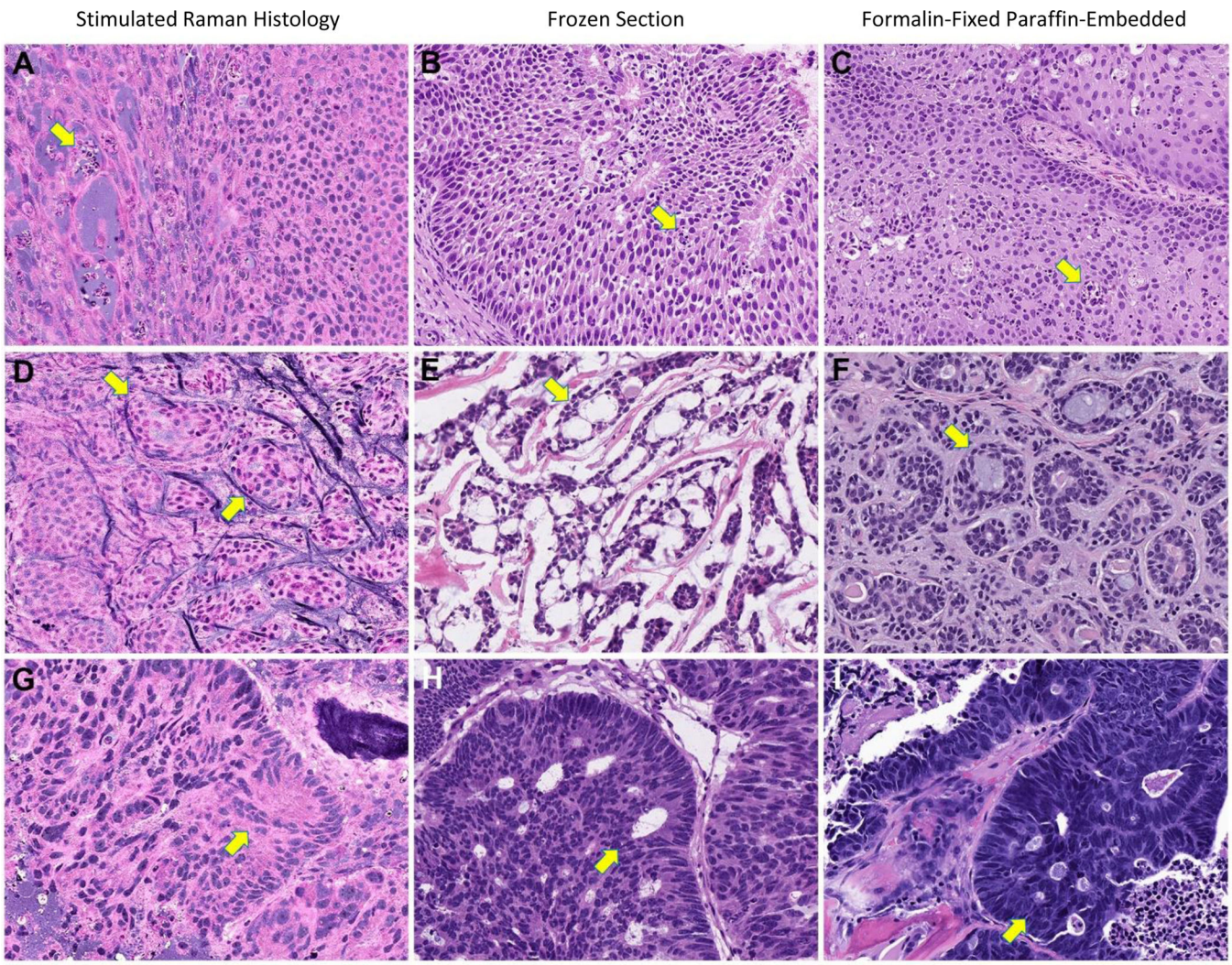

Figure 2:

Specific pathological features seen on stimulated Raman histology, frozen section, and formalin-fixed paraffin-embedded hematoxylin and eosin sections in sinonasal papilloma inverted type (panels A, B, C), adenoid cystic carcinoma (panels D, E, F) and metastatic colorectal adenocarcinoma (panels G, H, I).

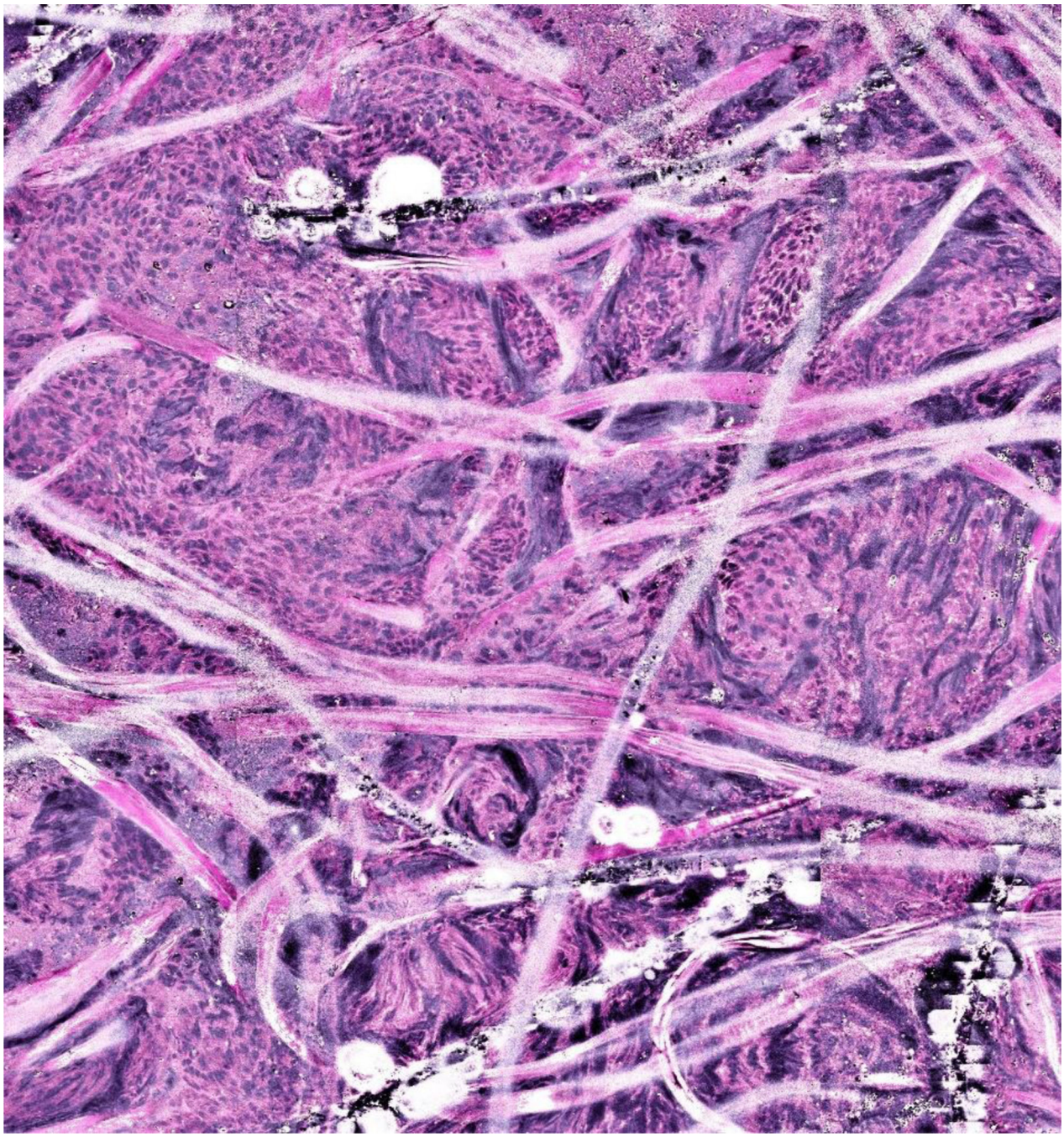

Figure 3:
Example of a stimulated Raman histology image with artifact due to handling error during processing.

Table 1:

Patient and tumor characteristics

Case	Age (years)	Sex	Pathology	Tumor Location	Approach	FS Samples	SRH Samples	SRH Sample time (mins/secs)	FS sample Time (mins)
1	74	F	Adenoid cystic carcinoma	Pterygopalatine fossa	Endoscopic	4	4	4.43 minutes (266 secs)	44mins
2	84	F	SCC	Maxillary sinus	Open	5	3	3.77 minutes (226 secs)	40mins
3	63	M	SMARCB1-deficient sinonasal carcinoma	Ethmoid sinus/orbit	Endoscopic	1	4	4 minutes (240 secs)	48mins
4	67	F	Inverted papilloma	Maxillary sinus	Open	1	4	4.97 minutes (298 secs)	53mins
5	71	F	Mucosal melanoma	Nasal cavity	Endoscopic	2	4	5.22 minutes (313 secs)	50mins
6	61	M	SCC	Maxillary sinus	Open	10	10	6 minutes (360 secs)	42mins
7	58	M	Metastatic adenocarcinoma	Sphenoid sinus	Endoscopic	2	3	5.53 minutes (332 secs)	37mins
8	54	M	SCC	Nasal cavity	Endoscopic	1	4	4.08 minutes (245 secs)	42mins
9	54	F	Rhabdomyosarcoma	Frontal sinus	Open	5	5	4.17 minutes (250 secs)	35mins
10	43	F	Rhabdomyosarcoma	Ethmoid sinus	Endoscopic	7	9	4.47 minutes (268 secs)	46mins
11	22	F	Meningioma	Nasal cavity	Endoscopic	3	5	3.93 minutes (236 secs)	45mins
12	65	F	Inverted papilloma/SCC	Frontal sinus	Combined	6	12	3.77 minutes (240 secs)	47mins